THE GEOLOGICAL SOCIETY OF AMERICA®

Controls on the formation of microbially induced sedimentary structures and biotic recovery in the Lower Triassic of Arctic Canada

Paul B. Wignall[1,†], David P.G. Bond[2], Stephen E. Grasby[3,4], Sara B. Pruss[5], and Jeffrey Peakall[1]
[1]*School of Earth and Environment, University of Leeds, Leeds LS2 9JT, UK*
[2]*Department of Geography, Geology and Environment, University of Hull, Hull HU6 7RX, UK*
[3]*Geological Survey of Canada, 3303 33rd Street N.W., Calgary, Alberta T2L 2A7, Canada*
[4]*Department of Geoscience, University of Calgary, 2500 University Dr. N.W., Calgary, Alberta T2N 1N4, Canada*
[5]*Department of Geosciences, Smith College, Northampton, Massachusetts 01063, USA*

ABSTRACT

Microbially induced sedimentary structures (MISS) are reportedly widespread in the Early Triassic and their occurrence is attributed to either the extinction of marine grazers (allowing mat preservation) during the Permo-Triassic mass extinction or the suppression of grazing due to harsh, oxygen-poor conditions in its aftermath. Here we report on the abundant occurrence of MISS in the Lower Triassic Blind Fiord Formation of the Sverdrup Basin, Arctic Canada. Sedimentological analysis shows that mid-shelf settings were dominated by deposition from cohesive sand-mud flows that produced heterolithic, rippled sandstone facies that pass down dip into laminated siltstones and ultimately basinal mudrocks. The absence of storm beds and any other "event beds" points to an unusual climatic regime of humid, quiet conditions characterized by near continuous run off. Geochemical proxies for oxygenation (Mo/Al, Th/U, and pyrite framboid analysis) indicate that lower dysoxic conditions prevailed in the basin for much of the Early Triassic. The resultant lack of bioturbation allowed the development and preservation of MISS, including wrinkle structures and bubble textures. The microbial mats responsible for these structures are envisaged to have thrived, on sandy substrates, within the photic zone, in oxygen-poor conditions. The dysoxic history was punctuated by better-oxygenated phases, which coincide with the loss of MISS. Thus, Permo-Triassic boundary and Griesbachian mudrocks from the deepest-water settings have common benthos and a well-developed, tiered burrow profile dominated by *Phycosiphon*. The presence of the intense burrowing in the earliest Triassic contradicts the notion that bioturbation was severely suppressed at this time due to extinction losses at the end of the Permian. The notion that Early Triassic MISS preservation was caused by the extinction of mat grazers is not tenable.

INTRODUCTION

The post-mass extinction world of the Early Triassic is often considered to represent an unusual time in Earth history when marine recovery from the Permo-Triassic mass extinction (PTME) was delayed by the prevalence of marine anoxia (Hallam, 1991; Twitchett and Wignall, 1996; Woods et al., 2007; Wignall et al., 2010, 2016; Grasby et al., 2013, 2016; Pietsch et al., 2014), and anachronistic facies better known from Cambrian and earlier times were well developed; especially carbonate microbialites (e.g., Bagherpour et al., 2017) and microbially induced sedimentary structures (MISS) in sandstones (Wignall and Twitchett, 1999; Pruss et al., 2004, 2005; Baud et al., 2007; Noffke, 2010). In recent years a broad range of sandstone bedding features have been related to the presence of microbial mats at the time of deposition. These comprise textured surfaces, including small-scale wrinkles and more regular, parallel rides, that reflect the original microtopography of the mat. They also include impressions of bubbles trapped beneath the mats, all of these features are generally grouped together as MISS (Noffke et al., 2001; Davies et al., 2016).

Only the shallowest waters provided better oxygenated settings and a refuge from the widespread, inimical conditions of the Early Triassic (Wignall et al., 1998; Beatty et al., 2008; Knaust, 2010; Chen et al., 2011; Song et al., 2013; Proemse et al. 2013). MISSs are rarely reported from such environments indicating their poor preservation potential, because the mats were either grazed, or they could not develop in the first place because of the unstable, burrowed sediment surfaces. In contrast, others have argued that Early Triassic open marine conditions were not unusually stressful (Hofmann et al., 2013; Vennin et al., 2015). Instead, the loss of bioturbators during the PTME is said to have been responsible for the preservation of fine lamination (Hofmann et al., 2015), and a reduction in the depth of the sediment mixed layer (Buatois and Mángano, 2011). In this scenario, geochemical evidence for sediment anoxia is attributed to a lack of irrigation by bioturbation (Hofmann et al., 2015). Davies et al. (2016) has also challenged the uniqueness of supposedly anachronistic "Precambrian" MISS and argued that they are in fact commonplace in shallow marine Phanerozoic settings; however most of their post-Cambrian examples are from peritidal or fluvial settings.

This study aims to provide the first sedimentological study of the type locations of all four Early Triassic substages that are found in the Sverdrup Basin of Arctic Canada (Ellesmere and Axel Heiberg islands). The ammonoid-defined age of the strata is independently assessed by constructing a chemostratigraphic record. Having established an age model, sedimentological context and redox variations, we then record and discuss the origin of the abundant MISS that occur in the basin. Finally, we evaluate the broader significance of these occurrences in the debates on the significance of Early Triassic facies and the nature of recovery from the PTME.

REGIONAL GEOLOGY OF STUDY AREA

Present-day outcrops of Sverdrup Basin strata lie in the northern-most part of Nunavut, Canadian High Arctic. The basin extends ~1000 km

†p.b.wignall@leeds.ac.uk.

GSA Bulletin; May/June 2020; v. 132; no. 5/6; p. 918–930; https://doi.org/10.1130/B35229.1; 10 figures; 1 table; published online 30 August 2019.

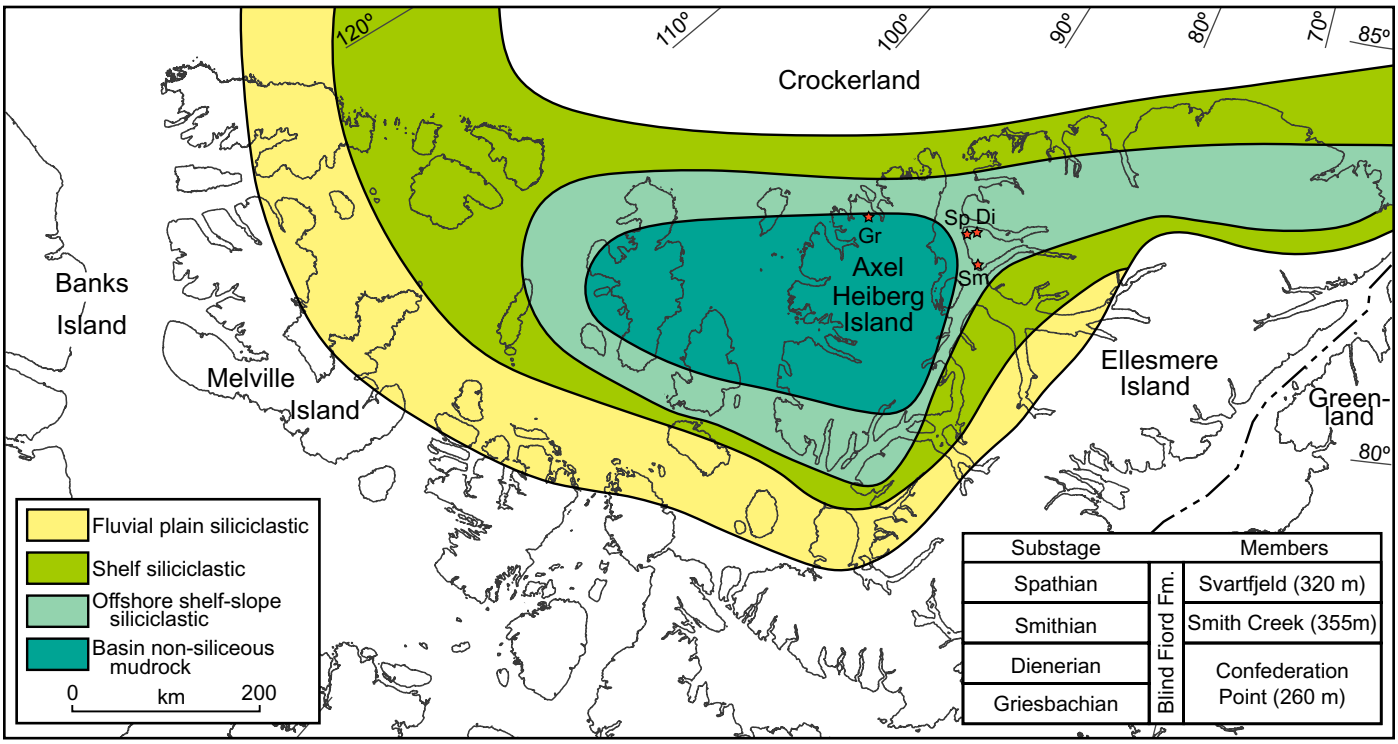

Figure 1. Regional paleogeography of the Sverdrup Basin, Arctic Canada, in the Early Triassic (from Embry and Beauchamp, 2008). Lower Triassic regional stratigraphy is given and thicknesses are those measured at Spath Creek/Cape St. Andrews. Red stars mark the field locations. Fm.—Formation.

east-west and 300 km north-south with its depocenter located in northern Ellesmere Island and Axel Heiberg Island (Fig. 1). The basin margins lay to the west, south, and east and opened to the northwest into the Boreal Ocean, although connection was limited due to the presence of Crockerland—an island or structural high that formed the northern basin rim (Embry, 1988, 1989, 2009; Fig. 1). Lower Triassic strata belong to the Blind Fiord Formation, a thick succession of offshore mudstone, siltstone, and shelf-slope sandstone that passes into paralic and terrestrial strata of the Bjorne Formation (Embry, 1988, 2009; Devaney, 1991; Embry and Beauchamp, 2008; Midwinter et al., 2017). The Blind Fiord Formation is divided into three members: the Confederation Point Member of Griesbachian to Dienerian age consists of heterolithic strata ranging from shale to sandstone; the Smith Creek Member of Smithian age consists of fine sandstone and siltstone; and the Svartfjeld Member of Spathian age consists of shale (Fig. 1). The Blind Fiord strata are arranged into a series of coarsening up/progradational packages punctuated by flooding events that saw expanded shale deposition. These can be correlated with transgressive-regressive cycles elsewhere in the world and are probably of eustatic origin (Embry, 1988, 1989). A latest Permian unconformity underlies the Blind Fiord Formation and cuts deeper into older Permian sediments toward the basin margins. Stable isotope studies show that the Blind Fiord Formation transgression occurred just prior to the PTME and that the sequence is conformable in the basin center (Grasby and Beauchamp, 2008). Shale deposition was most extensive in the basal Griesbachian, while the base of the Smith Creek Member (basal Smithian) and base of the Svartfjeld Member (basal Spathian) also mark major transgressions.

Study Sections

The four substages of the Early Triassic were established within the Blind Fiord Formation by Tozer (1965, 1967) and defined by their ammonoid content. His four type localities (Griesbach Creek, Diener Creek, Smith Creek, and Spath Creek continuing to Cape St. Andrews; Figs. 1 and 2) were the subject of our study during an expedition in July 2015. The basal 50 m of Confederation Point Member strata, with the exception of the unexposed basal-most meter, were logged in the western bank of Griesbach Creek on Axel Heiberg Island (Fig. 2). The other three sections lie on the Svartfjeld Peninsula, south of Otto Fiord in northwestern Ellesmere Island. The steep, eastern slopes of Spath Creek provide a series of near-continuous outcrops of the lower part of the Blind Fiord Formation, except for the basal 80 m which are covered. Our measured section began at N80° 54.464′ W89° 11.571′ (NAD83) in the upper part of the Confederation Point Member and continued to a level near the top of the Smith Creek Member where a major dolerite sill forms a prominent ridge. Logging was resumed to the northeast, at the same stratigraphic level (with some overlap), on the nearby slopes of Cape St. Andrews (N80° 55.072′ W89° 14.491′) and continued up to the lower beds of the Svartfjeld Member (Fig. 3). In addition to these two locations the same levels were also examined (and sampled) at Smith Creek and at Diener Creek (Fig. 2).

METHODS

Facies and Fossils

Sedimentary logging was undertaken through the basal 640 m of the Blind Fiord Formation at Griesbach Creek and Spath Creek to Cape St. Andrews, and facies were also examined and sampled at Diener and Smith Creeks (Fig. 3). Trace and body fossils were identified in the field and the intensity of bioturbation assessed using the semiquantitative ichnofabric index (II) scale of Droser and Bottjer (1986) which ranges from 1 (no burrows) to 5 (intense burrowing, no primary sedimentary structures preserved). The field observations were supplemented with analysis of 24 thin sections and polished slabs.

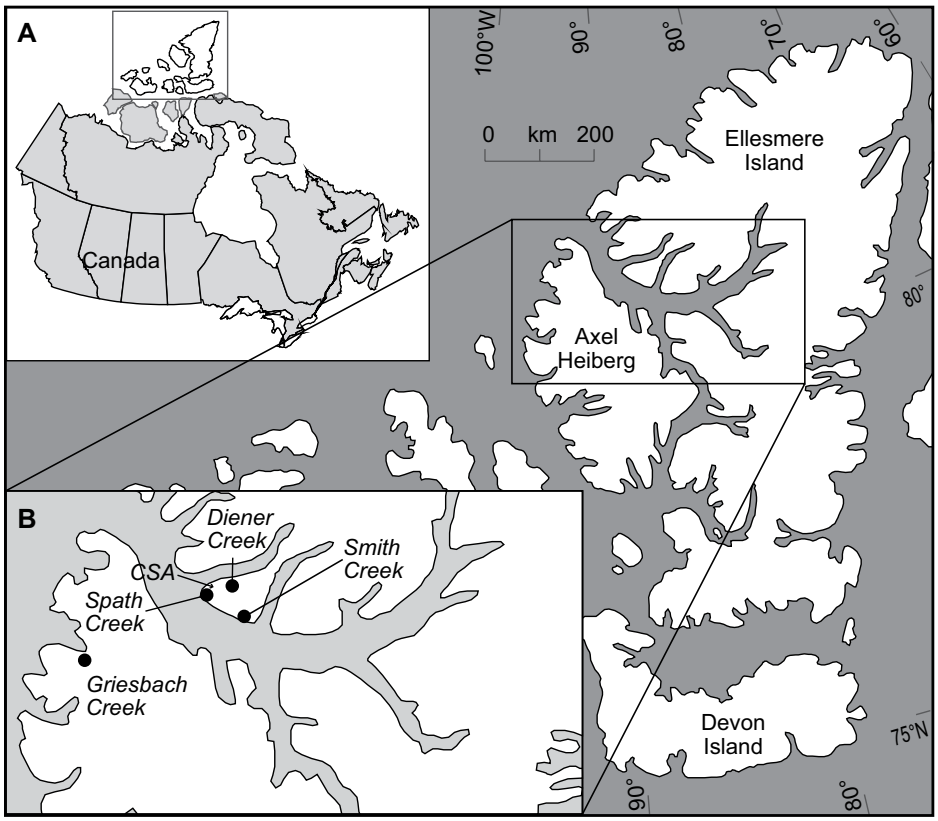

Figure 2. Location map of study sections from the central Sverdrup Basin, Arctic Canada.

Redox Proxies

The concentrations of redox-sensitive trace metals in marine strata provides a measure of ancient depositional conditions, because the reduced forms of many metals (e.g., molybdenum and uranium) are insoluble in seawater, with the result that these elements are scavenged under anoxic conditions. The U, Th, and K concentrations were measured in the field (generally every 3 m) using a Radiation Solutions RS-230 hand-held gamma ray spectrometer for 180 seconds that assays a parabola of rock ~1 m in diameter. One hundred and eleven samples from the same levels were taken for additional determinations of U, Mo, and Al concentrations at Acme Laboratory Vancouver, Canada, where powdered samples, digested in a 2:2:1:1 acid solution of H_2O-HF-$HClO_4$-HNO_3, were subsequently analyzed using a PerkinElmer mass spectrometer with ± 2% analytical error. The trace metal data was normalized for clastic content (Mo/Al, Th/U) in order to examine for fluctuations in trace metal concentrations due to redox changes. Our mass spectrometry data provide an independent test of the validity of field based, hand-held gamma-ray spectrometry, and the two curves are in remarkably close accordance (Fig. 4).

Pyrite framboid size analysis is a useful tool for reconstructing ancient redox conditions. In modern environments, pyrite framboids form in the narrow iron-reduction zone developed at the redox boundary, but they cease growing in the more intensely anoxic conditions of the underlying sulfate-reduction zone (Wilkin et al., 1996; Wilkin and Barnes, 1997). If bottom waters become euxinic (i.e., free H_2S occurs within the water column), then framboids develop in the water column but are unable to achieve diameters much larger than 5–6 µm before they sink below the iron reduction zone and cease to grow (Wilkin et al., 1996). Euxinic conditions are therefore characterized by populations of tiny framboids with a narrow size range whereas dysoxic/weakly oxygenated seafloors contain framboid populations that are larger and more variable in size (Bond and Wignall, 2010). Twenty-five samples from Griesbach Creek, Diener Creek, and Spath Creek-Cape St. Andrews were examined using carbon-coated polished chips viewed in backscatter mode at magnification ~×2500 under FEI Quanta 650 (at University of Leeds, Leeds, UK) and Zeiss EVO-60 (at University of Hull, Hull, UK) scanning electron microscopes to determine pyrite content, and where present, the size distribution of pyrite framboids. Where possible, at least 100 framboids were measured from each sample (levels bearing statistically robust numbers of pyrite framboids are shown on Fig. 3). Framboid size distributions are plotted with mean diameter versus standard deviation within each sample, which allows comparison of framboid populations in ancient sediments with modern euxinic, anoxic, and dysoxic populations (Bond and Wignall, 2010).

Chemostratigraphy

The same 111 samples taken for trace metal analysis from Spath Creek-Cape St. Andrews were also analyzed for their organic carbon isotope ($\delta^{13}C_{org}$) values. In addition, 26 samples from the basal part of the Griesbach Creek section were also analyzed. All samples were subject to continuous flow–elemental analysis–isotope ratio mass spectrometry in Calgary, Alberta, Canada, with a Finnigan Mat Delta + XL mass spectrometer interfaced with a Costech 4010 elemental analyzer, with standards run every fifth sample. Combined analytical and sampling error for $\delta^{13}C_{org}$ is ± 0.2‰ (1σ). The oscillations of $\delta^{13}C_{org}$ values in the Early Triassic provides a valuable chemostratigraphic age model (Grasby et al., 2013) that complements, and is independent of, Tozer's (1965, 1967) ammonoid-based biostratigraphy.

RESULTS AND INTERPRETATIONS

Stratigraphy

The basal part of the Confederation Point Member at Griesbach Creek begins with shale and coarsens upwards to siltstone (Fig. 3). For the most part these strata are blocky although platy siltstone is developed for 3.5 m beginning 6.0 m above the base of the section. In the uppermost part of the measured section, siltstone and tabular sandstone beds are interbedded and, above the level studied here, a further 20 m of sandstone and shelly limestone beds completes the coarsening-upward unit. The basal 20 m of the Confederation Point Member was also examined at Diener Creek where it comprised shale in the lower half that coarsens up to fissile siltstone.

A 180-m-thick section of the upper part of the Confederation Point Member was examined at Spath Creek. Sandstone dominates the succession although there are many siltstone levels as well as several unexposed stretches that are probably dominated by finer-grained strata based on the presence of shale and siltstone chips seen in the ex-situ scree material. A major (30 m-thick) sandstone forms the topmost part of the Member.

The transition between the Confederation Point and overlying Smith Creek members

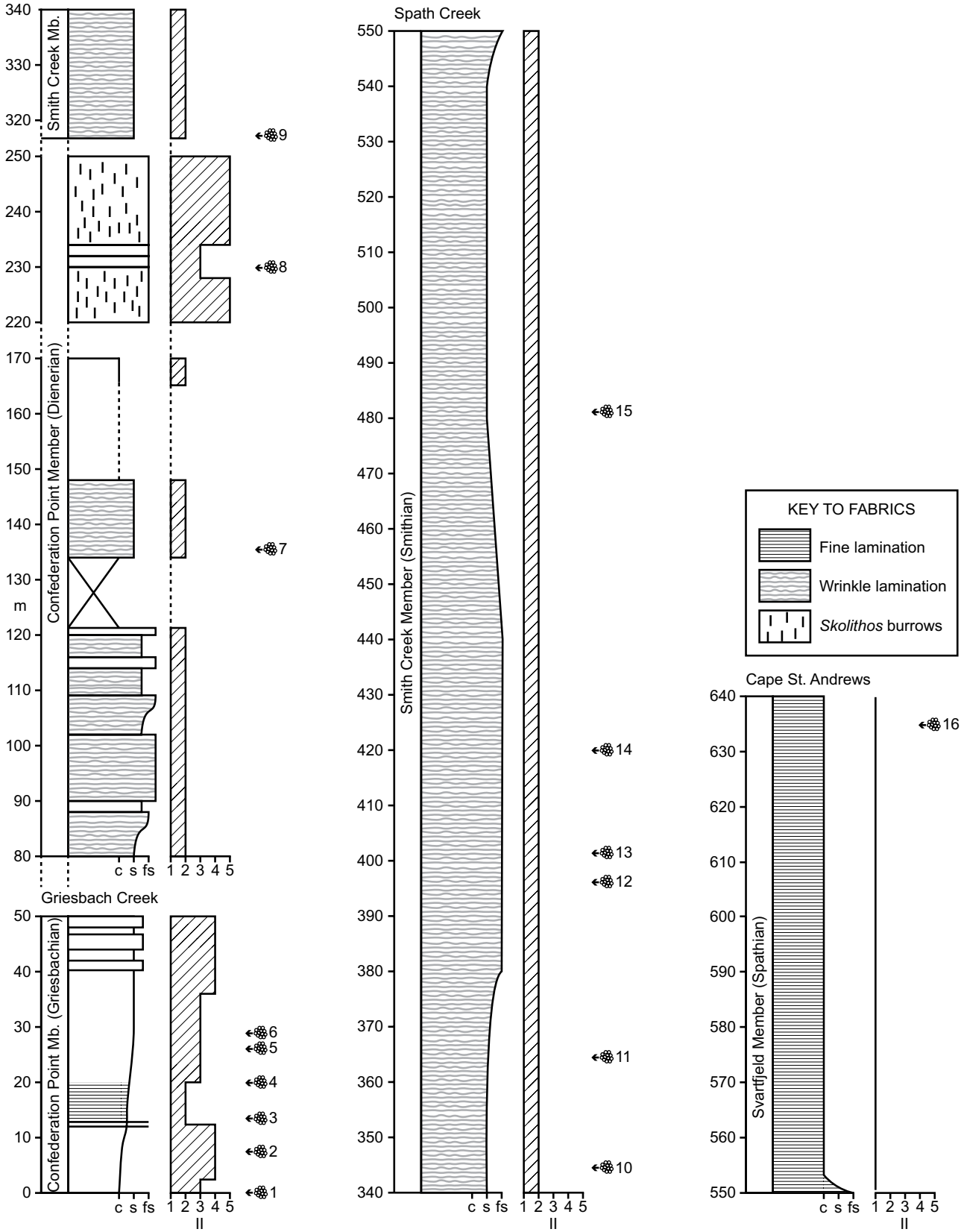

Figure 3. Composite stratigraphic log with sedimentary fabrics and ichnofabric index (II, after Droser and Bottjer, 1986) values through the lower part of the Blind Fiord Formation seen at Griesbach Creek, Spath Creek, and Cape St. Andrews (Arctic Canada). The position of samples analyzed for their pyrite framboid size distributions are marked and numbered 1–16 (see Fig. 9). Mb.—Member.

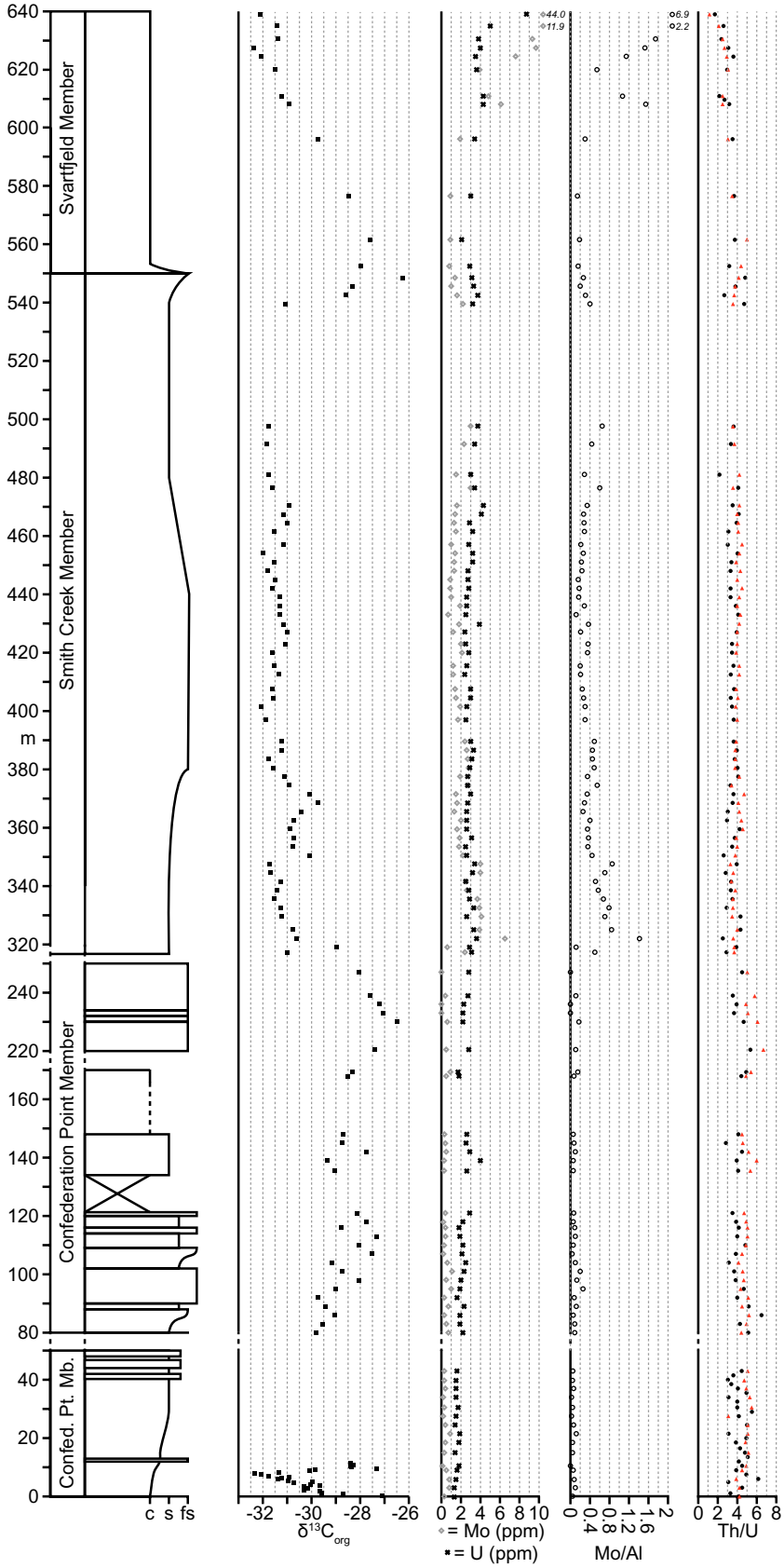

Figure 4. Carbon isotope values ($\delta^{13}C_{org}$) and trace metal redox proxies measured from the lower part of the Blind Fiord Formation seen at Griesbach Creek, Spath Creek, and Cape St. Andrews (Arctic Canada). The Th/U ratio (right hand panel) was measured in the field using a Radiation Solutions portable gamma-ray spectrometer (circles), while the triangles record values obtained on the same samples using inductively coupled plasma–mass spectrometry/emission spectroscopy. There is remarkable correspondence between the two curves, corroborating the application of field portable gamma-ray spectrometry. Confed. Pt. Mb.—Confederation Point Member; c—clay; s—sand; fs—fine sand.

occurs within a 70-m-thick unexposed interval at Spath Creek. This "gap" was examined at Smith Creek where thinly bedded sandstone strata were seen to dominate. The remainder of the Smith Creek Member is well exposed at Spath Creek and consists of gradual grain size fluctuations, on a scale of tens of meters, from siltstone to sandstone (Fig. 3). Superimposed on these changes are several levels where alternations of silty sandstone and sandy siltstone occur on a decimeter scale. Despite these subtle variations, weathering produces distinctive "banded" outcrops that are particularly well developed in the cliff sections on the western slopes of Diener Creek (Fig. 5).

The overlying, 320-m-thick Svartfjeld Member, seen immediately to the northeast of Spath Creek in the continuous section at Cape St. Andrews, is dominated by laminated shales. Prominent, yellow-weathering dolomite concretions and beds, and organic-rich shales are characteristic of the upper part of the member but not in the lower part considered here.

The ammonoid stratigraphy of the Blind Fiord Formation has primarily been based on collections from the same locations we have studied here (Tozer, 1965, 1967). The Dienerian/Smithian substage boundary was placed around the Confederation Point/Smith Creek contact and the Smithian/Spathian substage boundary around the contact between the Smith Creek and Svartfjeld members (Tozer, 1965, 1967). Our $\delta^{13}C_{org}$ data (Fig. 4) generally confirm these age assignments. Thus, in the upper Confederation Point Member there is a major decline of $\delta^{13}C_{org}$ values before they stabilize at –31‰ in the basal Smith Creek Member. A similar prolonged negative shift has also been reported at Smith Creek (Grasby et al., 2013) and in $\delta^{13}C_{carb}$ records from Tethys (e.g., Horacek et al., 2007; Korte and Kozur, 2010) where the onset of the negative excursion is placed in the early Smithian. Using this age assignment, the Dienerian/Smithian boundary probably lies in the upper part of the Confederation Point Member, a little lower than suggested by the ammonite records

Figure 5. Smith Creek Member outcrop seen on the western, upper slopes of Diener Creek, northern Svartfjeld Peninsula, northern Ellesmere Island showing decimeter-scale alternations between sandstone-rich and siltstone-rich levels. The subtle grainsize changes have been accentuated by weathering. David Bond for scale (1.85 m tall).

(which are rare and poorly preserved in this sandstone-dominated part of the section). The latest Smithian $\delta^{13}C_{org}$ data show a lowpoint followed by a rapid increase in both Smith Creek and in Tethyan locations (Fig. 4), in accord with the ammonoid biostratigraphy of this level.

The Permo-Triassic boundary is marked by a major negative C isotope excursion in sections throughout the world (e.g., Korte and Kozur, 2010). Our data from the lower part of Griesbach Creek also show a sharp negative excursion culminating in a low-point ~10 m from the base (Fig. 4). This suggests that the basal Blind Fiord Formation is of latest Permian age: an age assignment in agreement with the many recent studies of the boundary interval in the Sverdrup Basin (e.g., Grasby and Beauchamp, 2008; Baud et al., 2008; Beauchamp et al., 2009; Grasby et al., 2013, 2015).

Sedimentology

Several facies types occur within the Blind Fiord Formation.

Laminated Mudstone

Thinly laminated, silty mudstone is found in the lower part of the Confederation Point Member at Diener Creek (Fig. 2), and is commonly reported from the same level elsewhere in the Sverdrup Basin (e.g., Grasby and Beauchamp, 2008). This facies also forms a substantial thickness of strata in the lower part of the Svartfjeld Member in all sections.

The laminae are defined by fine silt-rich layers interbedded with clay and occur on a millimeter scale.

This low energy facies is interpreted to be the result of suspension-settling of clay minerals with regular, weak traction currents transporting silt grains to the depositional site. The absence of bioturbation suggests anoxic conditions.

Burrowed Mudstone

Most of the fine-grained strata of the Confederation Point Member at Griesbach Creek are bioturbated by millimeter diameter burrows of *Phycosiphon* that can form short vertical spirals, oblique to bedding. Dark, clay-rich material is concentrated in the burrow center surrounded by thicker haloes of very fine silt (Fig. 6A). Ichnofabric index varies from 3–4 in the burrowed mudstone and the most intensely bioturbated examples show a tiered profile of some complexity with *Phycosiphon* cross-cutting *Planolites* and in turn being cut by oblique burrows of *Catenichnus* (Fig. 6A). This facies type also has a considerable fossil content that includes common ammonoids, large bivalves (*Claraia*, *Modiolus*, *Unionites,* aviculopectinoids), bellerophontids, and bryozoans. The valves of the bivalves are often intensely bored.

We interpret this facies to record a low energy, well oxygenated depositional environment that allowed a diverse benthic fauna to thrive. By the standards of early Griesbachian mudrock environments (e.g., Dai et al., 2018), this is a rich fossil assemblage.

Laminated, Heterolithic Siltstone

This facies type is common in the upper part of the Confederation Point Member and throughout the Smith Creek Member where it dominates the 355-m-thick unit. It is mostly silt but the grain size ranges from clay through silt to very fine sand and is composed of both quartz and pyrite grains. Sedimentary structures include millimeter- to centimeter-scale planar laminae with most a few millimeters thick, but they can reach 1 cm (Fig. 6B). Both fining and coarsening upward trends are common within the laminae and thin beds. In the latter case the coarsest quartz sand and pyrite grains are concentrated in the uppermost part of the laminae and the top surfaces can be weakly eroded (Fig. 6B). Fossils are generally rare but include ammonoids and large *Claraia* up to 4 cm in height. Occasionally, *Claraia* populations, dominated by larval shells, can be prolific and cover bedding planes (Fig. 7A).

The repeated normal and reverse grading trends suggests waxing and waning of seafloor currents, an attribute often seen during deposition from hyperpycnal flows generated in shelf settings from river outflows that regularly surge and wane (Mulder et al. 2003; Wilson and Schieber, 2014). Deposition from hyperpycnal flows typically evolves from tractional to suspensional particularly as lofting occurs (Zavala et al., 2011; Steel et al., 2016), and the thicker mud laminae may record this process.

Heterolithic, Rippled Sandstone

This facies type shows thin bedding (1–2 cm thick), with fine scale alternation of sand, silt, and mud laminae, although sand-rich examples have few mud laminae. Ripple cross lamination is abundant (abundantly so in sand-rich developments of this facies: Fig. 8A) and flaser and lenticular bedded strata dominate when mud laminae are more common (Figs. 6C and 6D). Ripples generally show sinuous crests of the linguoid variety and can record migration over tens of centimeters, especially in sand-rich levels (Figs. 8A and 8B). Erosion surfaces/scours with a relief ranging from a millimeter up to (locally) two centimeters are common and overlying laminae either drape broad deflation surfaces or, in the case of the rippled strata, infill the scours (<2 cm deep) (Fig. 8A). Flow directions vary considerably, with the ripples in scours often migrating at a high angle to other ripples (Fig. 6C). Soft sediment deformation, in the form of minor loading, and centimeter-scale growth faults are also present (Figs. 6D and 8B).

The heterolithic, rippled sandstone beds have some attributes that are typically attributed to tidal settings: lenticular and flaser bedding with high-angle ripple flow directions (e.g., Reineck and Wunderlich, 1968; McCave, 1970; Allen, 1984). However, the paleogeographic occurrence of the Blind Fiord Formation in a semi-isolated basin (Fig. 1) is an unlikely setting for tidal activity: a microtidal regime would be anticipated. Also, contemporaneous nearshore/coastal facies show little evidence for tidal activity (Midwinter et al., 2017). The depositional processes recorded by this facies type (fine-scale alternations of ripples formed by traction currents, local scouring, and mud deposition) bear close comparison with experimental work on rapid deposition of mixtures of sand and mud (Baas et al., 2011, 2016). The presence of even small quantities of mud in a sand flow imparts some degree of cohesion to flow with the result that ripples form in a turbulent layer at the bed boundary while an overlying plug flow de-

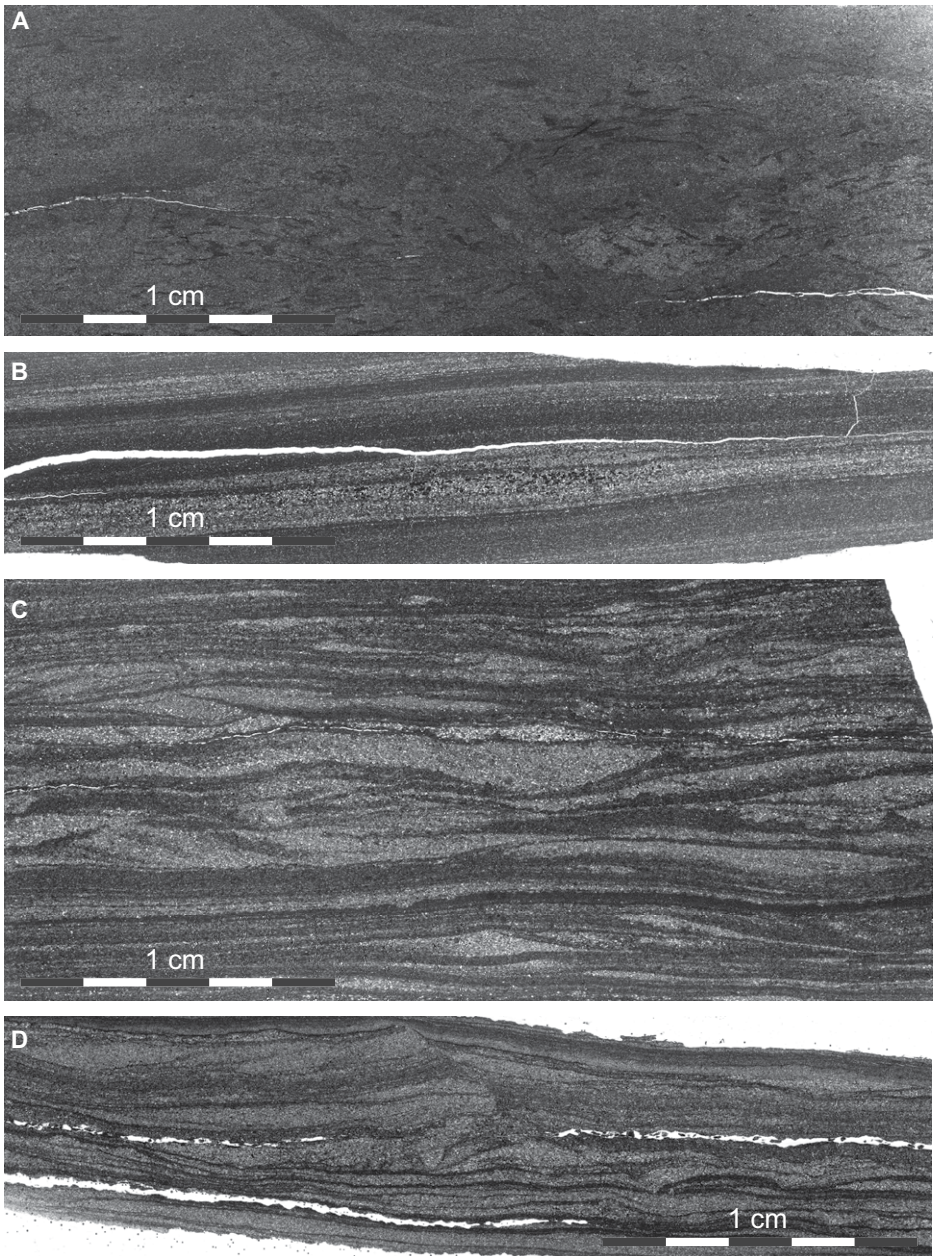

Figure 6. Scanned images of thin sections: (A) burrowed mudstone showing intense *Phycosiphon* bioturbation cross-cutting a diffuse, burrowed fabric of larger burrows that are probably horizontal *Planolites* and a single, oblique burrow of *Catenichnus*. Basal Griesbachian, Griesbach Creek, central Axel Heiberg Island; (B) laminated, heterolithic siltstone showing fine lamination and inverse grading in the two thickest laminae in which pyrite grains are concentrated in the upper parts. This is separated by a normal graded lamina. Smith Creek Member, Diener Creek, northern Svartfjeld Peninsula, northern Ellesmere Island; (C) heterolithic, rippled sandstone dominated by flaser bedding. Smith Creek Member, Diener Creek, northern Svartfjeld Peninsula, northern Ellesmere Island; and (D) heterolithic, rippled sandstone showing lenticular bedding, lamination and a small growth fault. Uppermost Smith Creek Member, Spath Creek, north-western Svartfjeld Peninsula, northern Ellesmere Island. All scale bars = 1 cm.

velops that ultimately deposits as a clay drape (Baas et al., 2016). Deposition thereby occurs as alternate laminae of cohesive and non-cohesive sediment with flow evolution often reaching the point where it can scour its own bed (Baas et al., 2011, 2016). The infill of scours often occurs with upstream facing laminae. All these features are seen in the heterolithic, rippled sandstones suggesting they were formed by decelerating mixed mud-sand flows with intrinsic depositional processes causing grain size segregation. Only recognized recently, such depositional conditions are probably common in the sedimentary record although bioturbation is likely to mask the depositional processes and produce homogenized, muddy sandstone in most cases. The Blind Fiord Formation examples are only weakly bioturbated to ichnofabric index 2 levels (Fig. 3) and burrows mostly consist of *Planolites* and rarer *Catenichnus* (Figs. 7C and 7D), probably due to prevailing dysoxic conditions on the seafloor (see below).

Skolithos Sandstone

The 30-m-thick, fine- to medium-grained sandstone that forms the top of the Confederation Point Member at Spath Creek shows bioturbation that ranges from intense (ichnofabric index 5) to weakly bioturbated, with a well-bedded level in its center (between 10 and 20 m in Fig. 3). Original sedimentary structures, now partly overprinted by burrows, were planar lamination and occasional ripples. The *Skolithos* burrows have an unusually narrow diameter for this ichnogenus (~2 mm) but can be up 20 cm in depth (Fig. 7B). They dominate the ichnofabric, and they cross-cut the horizontal burrows of *Planolites* and occasionally *Thalassinoides*. This facies also appears to have been important on the basin margin, in the Bjorne Formation, where Midwinter et al. (2017) record it as their facies association three (FA3), although the reported bioturbation intensity is less than seen in the Confederation Point Member and primary current lineation is well developed.

The abundant trace fossils suggest a fully marine, well-oxygenated environment with the dominance of vertical traces typical of nearshore deposition. This is the most proximal facies development in the Blind Fiord Formation. Midwinter et al. (2017) interpreted their FA3 as a braided stream deposit, albeit with a "weak marine influence" due to the trace fossil content. We suggest that the *Skolithos* sandstone in the Blind Fiord Formation formed in a marine-influenced, outer mouth bar setting where high current velocities produced primary current lineations.

Redox Conditions

Pyrite Framboid Analysis

Pyrite framboid size-frequency variations show a close correspondence with the facies of

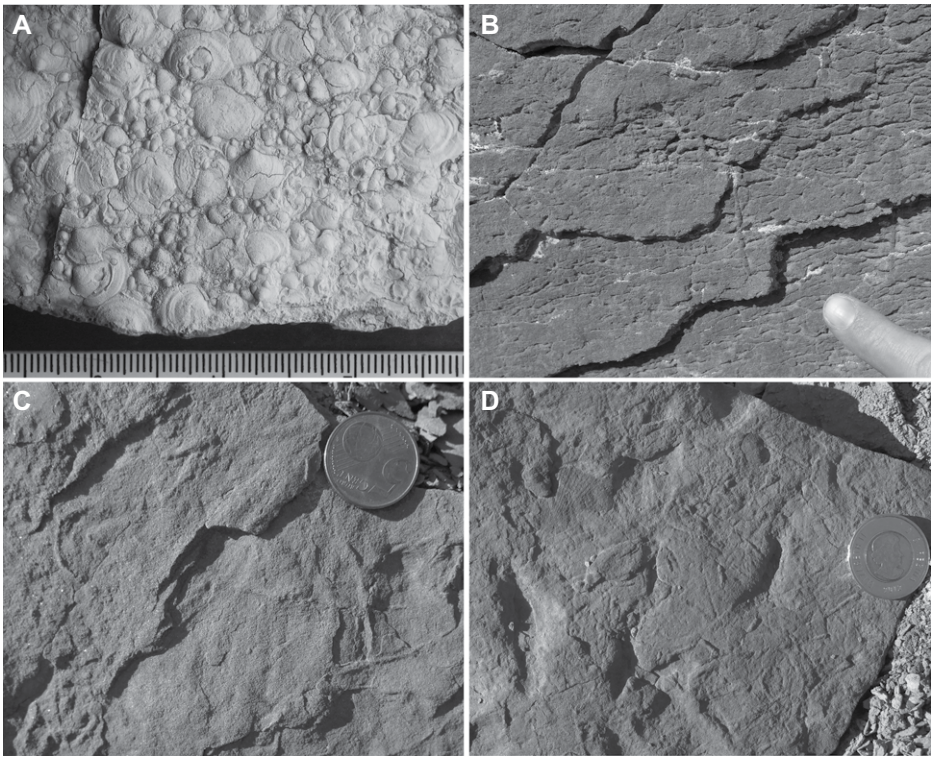

Figure 7. (A) Bedding planes covered in valves of *Claraia* dominated by larval shells but also with larger valves up to 15 mm in height. Upper Confederation Point Member, Spath Creek, north-western Svartfjeld Peninsula, northern Ellesmere Island. Ruler is marked in millimeters; (B) narrow (~2 mm wide) *Skolithos* burrows, uppermost Confederation Point Member, Spath Creek; (C) gently sinuous *Planolites* burrows, lower Smith Creek Member, Diener Creek, northern Svartfjeld Peninsula, northern Ellesmere Island. Coin is 21 mm in diameter; (D) short, straight *Planolites* burrows and *Claraia* valve. Possible *Catenichnus* burrows—shallow, broad U-shaped depressions picked out by the dark shadows—are also present; Smith Creek Member, Spath Creek, north-western Svartfjeld Peninsula, northern Ellesmere Island. Coin is 28 mm in diameter.

the Blind Fiord Formation. The lower Confederation Point Member at Griesbach Creek shows considerable variation of ichnofabric index (Fig. 3) and the lowest value (II2) occurs at a level that yields abundant pyrite framboids that plot in the anoxic field (sample 3, Figs. 3 and 9; Table 1). Most Griesbach Creek strata are moderately burrowed (II3–II4) and the associated framboids plot in the dysoxic field (samples 1, 2, 4, 5, and 6; Fig. 9; Table 1) indicating anoxia occurred within the sediment, while bottom waters were likely weakly oxygenated. The uppermost 15 m of the Griesbach Creek section consists of fully burrowed strata that lacks pyrite indicating well oxygenated conditions. In contrast, samples from the middle part of the Confederation Point Member, which occur in heterolithic siltstones and sandstones seen at the base of Spath Creek section (Fig. 3), are all pyrite rich and contain framboids that plot in the anoxic to dysoxic (mostly the latter) fields (Fig. 9; Table 1). The overlying *Skolithos* sandstone lacks pyrite indicating oxygenated conditions once again, which is perhaps not surprising given the intensity of bioturbation. A laminated (unbioturbated) interval within the *Skolithos* sandstone (sample 8) contains abundant framboids with a size-frequency distribution that plots in the dysoxic field despite the inferred shallow depositional depth (Fig. 9). The higher levels in the Blind Fiord Formation consist of heterolithic sandstones and siltstones with very little bioturbation (ichnofabric index 2) and abundant grains of pyrite including framboids that plot in the dysoxic field (Fig. 9).

In summary, the Blind Fiord Formation was, for the most part, deposited under oxygen-poor (dysoxic) conditions although prolonged intervals of much better ventilation are recorded in the Confederation Point Member, especially in the lower Griesachian strata. At times anoxia was even developed in nearshore conditions such as the laminated sandstones of the *Skolithos* facies. Interestingly, the oxygenated intervals do not link closely with facies or water depth because the best ventilation is recorded in both offshore, burrowed mudstone and the nearshore, deltaic *Skolithos* sandstone facies.

Trace Metal Concentrations

Concentrations of Mo and U, both absolute and normalized to Al and Th, respectively, provide a useful measure of redox conditions in ancient sediments (Tribovillard et al., 2006). Mo/U variations can also be informative because Mo enrichment occurs in euxinic conditions, when H_2S is present, and U uptake occurs under less intense redox conditions, at the Fe (II)–Fe (III) boundary (Wignall, 1994; Algeo and Tribovillard, 2009).

Molybdenum concentrations and Mo/Al ratios are low in the Confederation Point Member (<1 ppm and <0.4, respectively) and increase slightly in the Smith Creek and lower Svartfeld members before a major increase around 30 m above the base of the Svartfeld Member to 10 ppm and 1.8 (Fig. 4). Uranium concentrations show a similar trend to Mo whereas the Th/U ratio shows a gradual and persistent decline from ~5 at the base to <3 at the top of the Spath Creek section. The Th/U values from spectrometer field measurements and mass spectrometer assay give similar values (Fig. 4).

These results generally agree with the redox trend shown by the trace fossil and pyrite framboid studies presented above: overall better oxygenation in the Confederation Point Member succeeded by prevailing dysoxia at higher levels with anoxia/euxinia seen in the highest studied levels of the lower Svartfjeld Member.

Overview of Sverdrup Basin Environments

Depositional conditions within the Sverdrup Basin during the Early Triassic show many attributes typical of epicontinental basin fills: a "bulls-eye" style of facies belts with basinal mudrocks surrounded by silt and sand-dominated facies in shallower waters passing into a sandstone-dominated fluvial hinterland (Fig. 1; Embry and Beauchamp, 2008; Midwinter et al. 2017). Variations in the lateral extent of the facies is attributed to eustatic sea-level changes (Embry, 1988). Oxygenation levels were generally very low in the basin and dysoxic conditions occasionally expanded into shallow-water, nearshore environments. Unusually, the redox conditions do not link with these changes of base level. The best oxygenated intervals are seen in the basinal facies of the earliest Griesbachian,

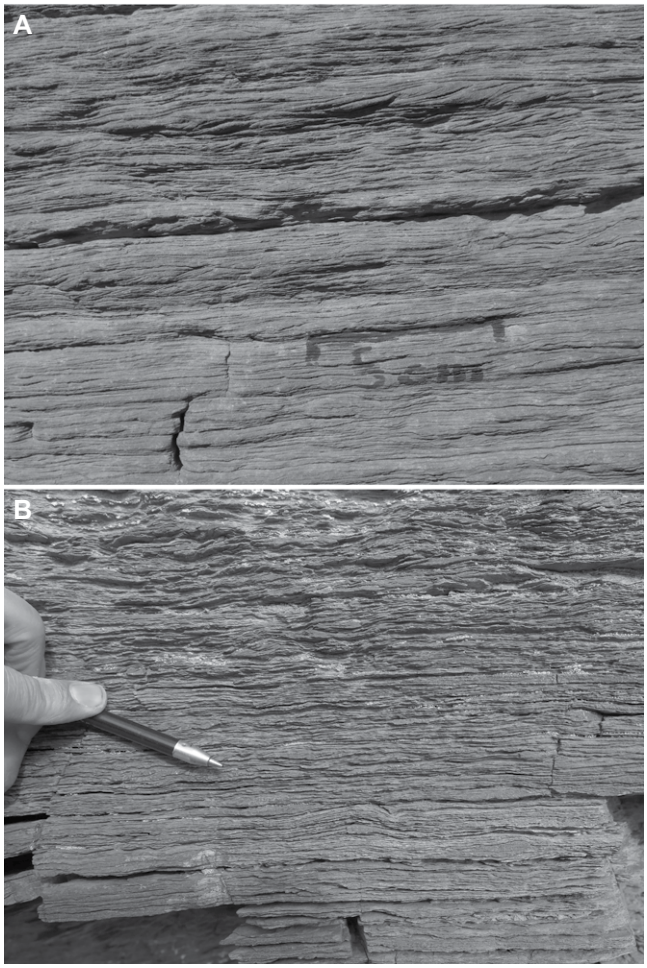

Figure 8. Field photographs of (A) heterolithic, rippled sandstone facies showing planar and ripple cross lamination. Erosion surfaces are present including an example at the center right that cuts down almost a centimeter. The hand-drawn scale bar on the outcrop is 5 cm long. Smith Creek Member, Diener Creek, northern Svartfjeld Peninsula, northern Ellesmere Island; and (B) heterolithic, rippled sandstone in which the abundance of silt laminae increases in the upper part. The pen points toward a tiny growth fault. Smith Creek Member, Spath Creek, north-western Svartfjeld Peninsula, northern Ellesmere Island.

a time of rapid transgression, and the nearshore facies of the mid Dienerian. A similar style of redox fluctuations is seen in the Boreal shelf setting of Spitsbergen, Norway, where anoxic conditions repeatedly developed in very shallow waters regardless of base-level fluctuations (Wignall et al., 2016).

There is remarkably little evidence for basinal processes in the Blind Fiord Formation. Wave ripples are essentially unknown, even in the nearshore strata recorded here and by Midwinter et al. (2017). Evidence for storm deposition is also lacking; the sedimentary record consists of continuous deposition of thin laminae with no thicker "event beds." This is despite the considerable fetch of the basin which may have reached 1000 km in extent (Fig. 1). The lack of storm facies is likely to record an unusual Early Triassic climatic regime. It is notable that the Lower Triassic strata of Spitsbergen were deposited at a similar latitude (~45°N) on an ocean-facing shelf and record only minor, rare storm events (Wignall et al., 2016).

The sediment discharge into the Sverdrup Basin was both intense and remarkably continuous. The Early Triassic succession at Spath Creek generally records accumulation in an outer shelf location and reaches nearly 950 m thickness. Taking an estimated 5 million year duration of deposition, gives an impressive sedimentation rate of 190 m/million years and indicates considerable run-off. At no point do individual bed thicknesses exceed a few centimeters indicating repeated minor discharges in a humid regime rather than a more flashy, semi-arid style of run-off. The common decimeter scale alternations of siltstone-dominated and sandstone-dominated deposition (Fig. 5) also indicate longer term variations of climate. These were likely on shorter timescales than Milankovitch cycles. Given the thickness noted above, these are likely to reflect run-off variations of ~1000 years frequency.

Having established the depositional regime within the Sverdrup Basin we now present and discuss the abundant MISS occurrences found in the Blind Fiord Formation. These mostly occur on bedding surfaces of the heterolithic, rippled sandstone facies with occasional examples in the laminated, heterolithic siltstones.

Microbially Induced Sedimentary Structures

Wrinkle Structures

Bedding surfaces of the heterolithic, rippled sandstone facies can be smooth, planar, or rippled but the majority show dense, irregular, linear, and gently curving wrinkle structures up to a centimeter in width with an amplitude of a few millimeters (Figs. 10B and 10C). The wrinkle structures sometimes show a consistent trend including sets with a crescentic pattern reminiscent of backfill in trace fossils like *Zoophycos* (Fig. 10D); however, they lack the outer ventilation shaft, characteristic of such fodinichnial burrows. These wrinkles are not directly comparable with "elephant skin" textures, that are typically cuspate in cross section with sharp ridges separating the cusps (Bottjer and Hagadorn, 2007; Gehling and Droser, 2009). The Blind Fiord Formation wrinkles show gently rounded cross sections that resemble the "mat deformation structures" illustrated by Porada and Bouougri (2007), the "large-scale irregular wrinkles" of Noffke (2000) and the "weave fabric" of Gehling and Droser (2009), a variety of their textured organic surface. The wrinkled surfaces are associated with patches of a finely dimpled texture, called "pucker" in Gehling and Droser (2009). Trace fossils are also occasionally seen: these have a much sharper definition than the wrinkles, and consist of short horizontal burrows of *Planolites* that cross-cut the wrinkles (Fig. 7C).

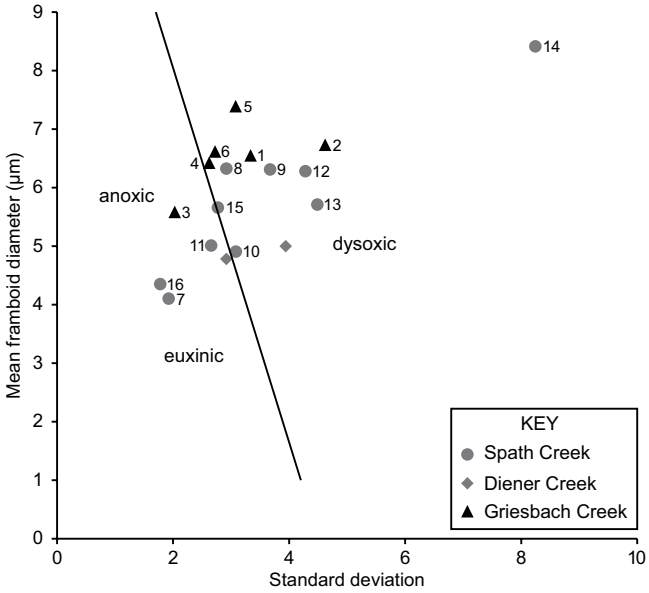

Figure 9. Plots of mean framboid diameter versus standard deviation for Blind Fiord Formation samples from Arctic Canada. The separation of the euxinic-anoxic field from the anoxic-dysoxic field is based on data from modern environments that span this range of oxygenation regimes (Bond and Wignall, 2010). Numbers represent sample levels shown in Figure 3.

Kinneyia

Kinneyia is a form of MISS consisting of reticulate patterns with sub-parallel, flat-topped ridges (Hagadorn and Bottjer, 1999; Pflüger, 1999). These are occasionally found in the heterolithic, rippled sandstones of the Confederation Point Member at both Smith Creek and Spath Creek (Fig. 10A), and are rarer than the wrinkle structures described above.

Bubble Texture

Also common on fine sandstone bedding surfaces are millimeter-sized hemispherical domes preserved in both positive and negative relief (Fig. 10E). They occur both in high density, where bubbles are regularly in contact, or as isolated bubbles. Occasional examples appear to have collapsed/burst and show either a central dimple, producing a concentric pattern, or crater. All these features are seen in both ancient (Dornbos et al., 2007) and modern microbial mats where they are caused by trapping of gas bubbles that occasionally escape and "burst" through mats (Davies et al., 2016).

TABLE 1. PYRITE FRAMBOID SIZE DISTRIBUTIONS FROM STUDY SECTIONS ON AXEL HEIBERG AND ELLESMERE ISLANDS, NUNAVUT, CANADIAN HIGH ARCTIC

Sample	Height in section (m)	N	Mean diameter (μm)	Standard deviation	Min diameter (μm)	Max diameter (μm)
1	0	109	6.55	3.34	1.5	22
2	7.5	112	6.73	4.62	2.5	37.5
3	13.5	106	5.58	2.03	2	11
4	20	107	6.43	2.62	2	25.5
5	26	84	7.39	3.08	3	22.5
6	29	106	6.62	2.72	1.5	15.5
7	135.5	107	4.10	1.92	1.5	12.5
8	230	57	6.32	2.92	2.5	15.5
9	316	103	6.31	3.67	2	29
10	344.5	96	4.91	3.08	1	18.5
11	365.5	96	5.01	2.66	2	18
12	397	57	6.28	4.28	1.5	26.5
13	401.5	105	5.71	4.49	1.5	33
14	420	138	8.41	8.24	2.5	68
15	481	111	5.66	2.77	1.5	15.5
16	635	112	4.35	1.78	1	15
Diener Creek, DC1	n/a	129	5.00	3.94	1.5	30
Diener Creek, DC3	n/a	102	4.78	2.92	1.5	15

Notes: N—number of framboid counts per sample. Samples positions are shown in Figure 3.

Controls of MISS Occurrences in the Early Triassic

The abundance of MISS, associated with low intensity burrowing, in the Blind Fiord Formation is a feature more typical of the Ediacaran Period (e.g., Gehling and Droser, 2009). Phanerozoic occurrences, including microbial structures (Noffke et al., 2001), occur over a limited depth range in the offshore transition zone, and require low oxygen conditions to suppress bioturbation and mat grazing (Pflüger, 1999; Mata and Bottjer, 2009). The Sverdrup surfaces are similarly associated with intermediate water depths, where low oxygen conditions prevailed. They are not found in the intensely bioturbated, *Skolithos* sandstone shoreface facies nor in the deeper water mudstone facies, which can be burrowed or laminated. The MISS disappear at the base of the Spathian, which saw transgression and intensification of oxygen restriction, likely due to deepening below the photic zone at this level. Thus, it appears that both redox conditions and a water depth within the photic zone control MISS occurrences in the Early Triassic. A similar discrete, depth occurrence is seen for microbial mat occurrences in the Neoproterozoic which was favored at shallow water depths (i.e., in the photic zone) in siliciclastic settings where episodic influx of sand and finer sediment favored growth and then burial of mats (Noffke et al., 2002).

Davies et al. (2016) have argued that the reported prevalence of microbial surfaces in the Early Triassic (e.g., Pruss et al., 2004; Chu et al., 2017) is an artifact of over-sampling from this interval, and that they are probably a mundane facet of Phanerozoic conditions. They supported their contention with a survey that highlighted many MISS occurrences. However, most of the post-Cambrian occurrences described in Davies et al. (2016) are from lacustrine or peritidal environments. The examples from the Early Triassic of the Sverdrup Basin are clearly atypical Phanerozoic facies because they are found in an open marine setting. The poorly oxygenated seafloor conditions suppressed burrowing organisms and ensured the preservation of the microbial mats. The mats presumably developed quickly because sedimentation (from flows of cohesive sand-mud mixtures) was frequent. Dysoxic, shelf facies are not uncommon in the Phanerozoic, but these are usually developed in mudstone facies whereas the MISS occurrences of the Blind Fiord Formation are in sandstones.

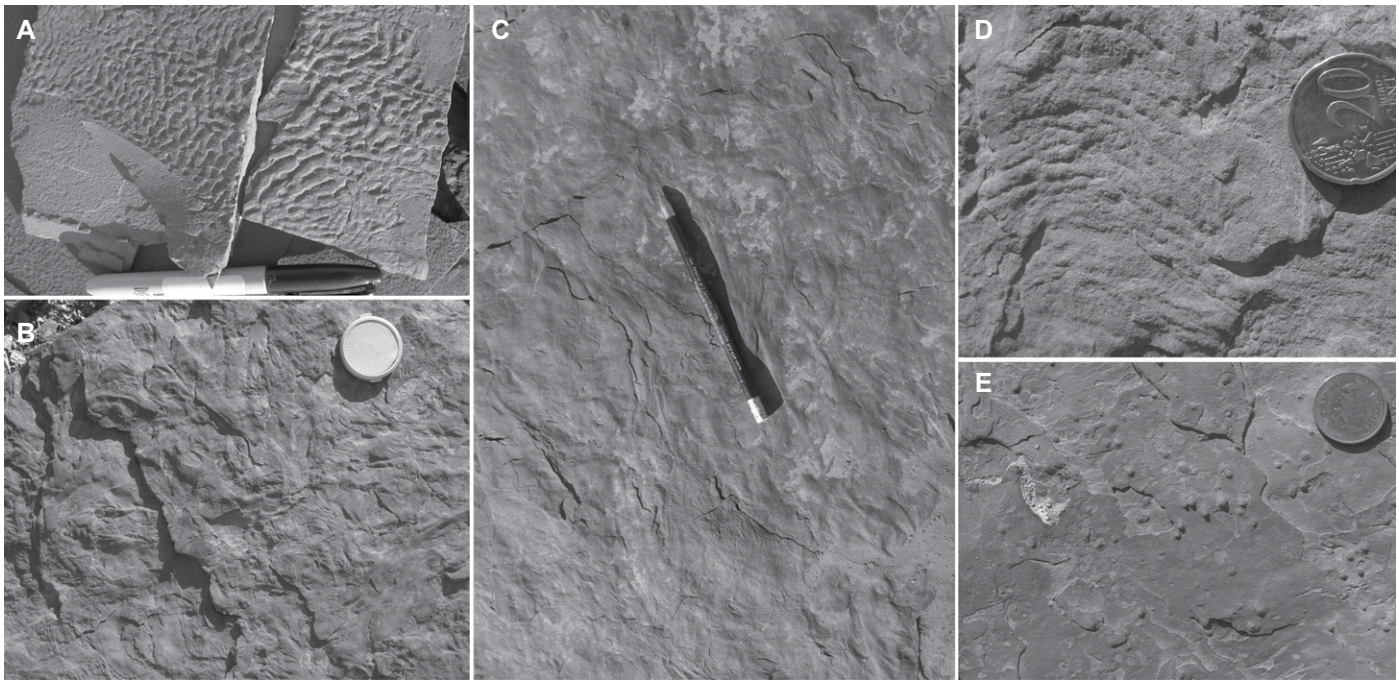

Figure 10. Microbially induced sedimentary structures from the Lower Triassic of Ellesmere Island (Arctic Canada): (A) Sandstone slabs showing *Kinneyia* mat structures, Smith Creek Member, Spath Creek; pen is 13 cm in length; (B) bedding surface of sandstone showing complete coverage of wrinkles. Lens cap is 5 cm in diameter. Smith Creek Member, Diener Creek; (C) bedding surface with wrinkle structures and a fine, puckered appearance in the center of the field of view. Pen for scale. Smith Creek Member, Diener Creek; (D) wrinkle structures in stacked crescentic pattern recalling trace fossil backfill structure. Coin is 22 mm in diameter. Smith Creek Member, Diener Creek; and (E) isolated bubble marks seen on the lower surface of a laminated slab of sandstone. Lower Smith Creek Member, Smith Creek. Coin is 23 mm in diameter.

This suggests that, for MISS to develop in the Phanerozoic, an ideal taphonomic window (cf. Noffke et al., 2002) requiring both dysoxia and sandy substrates was necessary.

Recovery in the Early Triassic

The bioturbation seen in the Blind Fiord Formation has a bearing on models for the recovery of marine communities in the aftermath of the PTME. It has been argued that the Early Triassic recovery of bioturbators was slow (spanning several million years), and stepwise with a progressive increase in burrow size, depth, and tiering complexity (Twitchett, 2006; Chen et al., 2011). However, there are several examples that contradict this notion. Complex, tiered trace fossil communities were developed immediately after the PTME in shallow-water Griesbachian settings of western Canada (Beatty et al., 2008), northern Italy (Hofmann et al., 2011) and in the shoreface and offshore, basinal settings of Ellesmere and Axel Heiberg islands recorded here. While severe, the Permo-Triassic mass extinction clearly did not eliminate mobile infauna and plenty remained to burrow to a range of depths. In the Sverdrup Basin, offshore mudstone contains tiered profiles that record burrow depths of at least ~3 cm while shoreface *Skolithos* burrows achieved depths of 20 cm. Thus, trace fossil tiering complexity does not provide a good measure of the recovery rates. Local benthic oxygenation levels are the main control on bioturbation and the resulting ichnofabrics rather than the time elapsed since the extinction.

The link between oxygenation and bioturbation is reversed in the model of Hofmann et al. (2015). They argued that the extinction of most bioturbators at the end of the Permian resulted in weakly bioturbated sediments in the Early Triassic that consequently saw anoxic conditions develop close to the sediment surface. Thus, "phenomena that are commonly interpreted as evidence for Early Triassic seawater anoxia may have been caused by the extinction of burrowers" (Hofmann et al., 2015, p. 10). Hofmann et al. (2015) recognized that bioturbated strata are in fact present after the mass extinction, indeed they have recorded examples of burrows themselves (Hofmann et al., 2011), but this evidence is dismissed because the burrowers supposedly only belong to shallow, infaunal guilds. However, our examples show that earliest Griesbachian offshore mudstone horizons have a mixed layer with well-developed tiering. Such ichnofabrics are lost at younger levels of the Blind Fiord Formation where more intense oxygen restriction was prevalent. Thus, dysoxia, not an absence of bioturbators, inhibited bioturbation in the Early Triassic of the Sverdrup Basin.

CONCLUSION

The Early Triassic history of the Sverdrup Basin was highly unusual. The absence of storm beds indicates generally low energy conditions. Sedimentation was dominated by a near-continuous run-off of cohesive flows of sand-mud mixtures that produced distinctive heterolithic strata in mid-shelf settings that passed offshore to siltstones and ultimately mudstones. Dysoxic seafloor conditions predominated, and often extended into shallow water, but oxygenation levels varied considerably. During the earliest Griesbachian conditions were only weakly dysoxic and a tiered burrow profile developed; an unusual occurrence in the immediate aftermath of the Permo-Triassic mass extinction that contradicts claims that the extinction of burrowing organisms caused weak bioturbation at this time.

The dysoxic, mid-water depths of the Sverdrup Basin saw the prolonged accumulation of heterolithic, rippled sandstone and siltstone with bedding surfaces that show abundant evidence

for microbial mats (wrinkle structures, *Kinneyia*, and gas bubbles). The key requirements for this MISS development were a specific set of conditions: fine sand substrates, dysoxic bottom waters and moderate water depths within the photic zone. Such conditions were unusual in the Phanerozoic, but their widespread presence in Ellesmere Island, and more widely in the Early Triassic, is a reflection of the unusual environmental conditions of this post-extinction world and not, as has been claimed by some, due to the magnitude of the preceding extinction losses.

ACKNOWLEDGMENTS

The Geological Survey of Canada for funding fieldwork through its High Arctic Large Igneous Province project, and the Natural Environment Research Council for additional financial support (grant NE/J01799X/1 to DPGB). Natural Resources Canada's Polar Continental Shelf Program in Resolute, Nunavut, Canada, provided valuable logistical support. We thank Deirdra Stacey for her assistance during field sampling. Mark Anderson prepared thin sections and polished chips, and Tony Sinclair assisted with scanning electron microscope work in Hull, UK. Finally, we thank the pilots of Kenn Borek Air and Universal Helicopters Newfoundland and Labrador, Canada for providing safe passage around the Arctic, and the staff of Eureka Weather Station for their hospitality pre- and post-fieldwork. We also thank the editor and reviewers for their useful comments and suggestions.

REFERENCES CITED

Algeo, T.J., and Tribovillard, N., 2009, Environmental analysis of paleoceanographic systems based on molybdenum-uranium covariation: Chemical Geology, v. 268, p. 211–225, https://doi.org/10.1016/j.chemgeo.2009.09.001.

Allen, J.R.L., 1984, Sedimentary Structures: Their Character and Physical Basis: Amsterdam, The Netherlands, Elsevier, 663 p.

Baas, J.H., Best, J.L., and Peakall, J., 2011, Depositional processes, bedform development and hybrid bed formation in rapidly decelerated cohesive (mud-sand) sediment flows: Sedimentology, v. 58, p. 1953–1987, https://doi.org/10.1111/j.1365-3091.2011.01247.x.

Baas, J.H., Best, J.L., and Peakall, J., 2016, Predicting bedforms and primary current stratification in cohesive mixtures of mud and sand: Journal of the Geological Society, v. 173, p. 12–45, https://doi.org/10.1144/jgs2015-024.

Bagherpour, B., Bucher, H., Baud, A., Brosse, M., Vennemann, T., Martini, R., and Guodon, K., 2017, Onset, development, and cessation of basal Early Triassic microbialites (BETM) in the Nanpanjiang pull-apart Basin, South China Block: Gondwana Research, v. 44, p. 178–204, https://doi.org/10.1016/j.gr.2016.11.013.

Baud, A., Richoz, S., and Pruss, S., 2007, The lower Triassic anachronistic carbonate facies in space and time: Global and Planetary Change, v. 55, p. 81–89, https://doi.org/10.1016/j.gloplacha.2006.06.008.

Baud, A., Nakrem, H.A., Beauchamp, B., Beatty, T.W., Embry, A.F., and Henderson, C.M., 2008, Lower Triassic bryozoan beds from Ellesmere Island, High Arctic, Canada: Polar Research, v. 27, p. 428–440, https://doi.org/10.1111/j.1751-8369.2008.00071.x.

Beatty, T.W., Zonneveld, J.P., and Henderson, C.M., 2008, Anomalously diverse Early Triassic ichnofossil assemblages in northwest Pangea: A case for a shallow-marine habitable zone: Geology, v. 36, p. 771–774, https://doi.org/10.1130/G24952A.1.

Beauchamp, B., Henderson, C.M., Grasby, S.E., Gates, L.T., Beatty, T.W., Utting, J., and James, N.P., 2009, Late Permian sedimentation in the Sverdrup Basin, Canadian Arctic: The Lindstrom and Black Stripe Formations: Bulletin of Canadian Petroleum Geology, v. 57, p. 167–191, https://doi.org/10.2113/gscpgbull.57.2.167.

Bond, D.P.G., and Wignall, P.B., 2010, Pyrite framboid study of marine Permo-Triassic boundary sections: A complex anoxic event and its relationship to contemporaneous mass extinction: Geological Society of America Bulletin, v. 122, p. 1265–1279, https://doi.org/10.1130/B30042.1.

Bottjer, D., and Hagadorn, J.W., 2007, Mat features in sandstones, *in* Schieber, J., Bose P., Eriksson, P.G., Banerjee, S., Sarkar, S., Altermann, W., and Catuneanu, O., eds., Atlas of Microbial Features Preserved within the Siliciclastic Rock Record, Volume 2: Amsterdam, The Netherlands, Elsevier, p. 53–71.

Buatois, L.A., and Mángano, M.G., 2011, The déjà vu effect: Recurrent patterns in exploitation of ecospace, establishment of the mixed layer, and distribution of matgrounds: Geology, v. 39, p. 1163–1166, https://doi.org/10.1130/G32408.1.

Chen, Z.Q., Tong, J.N., and Fraiser, M.L., 2011, Trace fossil evidence for restoration of marine ecosystems following the end-Permian mass extinction in the Lower Yangtze region, South China: Palaeogeography, Palaeoclimatology, Palaeoecology, v. 299, p. 449–474, https://doi.org/10.1016/j.palaeo.2010.11.023.

Chu, D.L., Tong, J.N., Bottjer, D.J., Song, H.J., Song, H.Y., Benton, M.J., Tian, L., and Guo, W.W., 2017, Microbial mats in the terrestrial Lower Triassic of North China and implications for the Permian-Triassic mass extinction: Palaeogeography, Palaeoclimatology, Palaeoecology, v. 474, p. 214–231, https://doi.org/10.1016/j.palaeo.2016.06.013.

Dai, X., Song, H.J., Wignall, P.B., Jia, E.H., Bai, E.H., Wang, F.Y., Chen, J., and Tian, Li., 2018, Rapid biotic rebound during the late Griesbachian indicates heterogeneous recovery patterns after the Permian-Triassic mass extinction: Geological Society of America Bulletin, v. 130, p. 2015–2030, https://doi.org/10.1130/B31969.1.

Davies, N.S., Liu, A.G., Gibling, M.R., and Miller, R.F., 2016, Resolving MISS conceptions and misconceptions: A geological approach to sedimentary surface textures generated by microbial and abiotic processes: Earth-Science Reviews, v. 154, p. 210–246, https://doi.org/10.1016/j.earscirev.2016.01.005.

Devaney, J.R., 1991, Sedimentological highlights of the Lower Triassic Bjorne Formation, Ellesmere Island, Arctic Archipelago: Current Research: Geological Survey of Canada, Paper 91-1B, p. 33–40.

Dornbos, S.Q., Noffke, N., and Hagadorn, J.W., 2007, Matdecay features, *in* Schieber, J., Bose P., Eriksson, P.G., Banerjee, S., Sarkar, S., Altermann, W., and Catuneanu, O., eds., Atlas of Microbial Features Preserved within the Siliciclastic Rock Record, Volume 2: Amsterdam, The Netherlands, Elsevier, p. 106–110.

Droser, M.L., and Bottjer, D.J., 1986, A semiquantitative field classification of ichnofabric: Research method paper: Journal of Sedimentary Research, v. 56, p. 558–559, https://doi.org/10.1306/212F89C2-2B24-11D7-8648000102C1865D.

Embry, A.F., 1988, Triassic sea-level changes: Evidence from the Canadian Arctic Archipelago, *in* Wilgus, C.K., Hastings, B.S., Posamentier, H., Wagoner, J.V., Ross, C.A., and Kendall, C.G.St.C., eds., Sea-Level Changes: An Integrated Approach: Tulsa, Oklahoma, USA, Society of Economic Paleontologists and Mineralogists Special Publication 42, p. 249–259, https://doi.org/10.2110/pec.88.01.0249.

Embry, A.F., 1989, Correlation of Upper Palaeozoic and Mesozoic sequences between Svalbard, Canadian Arctic Archipelago, and northern Alaska, *in* Collinson, J.D., ed., Correlation in Hydrocarbon Exploration: Dordrecht, The Netherlands, Springer, p. 89–98, https://doi.org/10.1007/978-94-009-1149-9_9.

Embry, A., 2009, Crockerland: The source area for the Triassic to Middle Jurassic strata of Northern Axel Heiberg Island, Canadian Arctic Islands: Bulletin of Canadian Petroleum Geology, v. 57, p. 129–140, https://doi.org/10.2113/gscpgbull.57.2.129.

Embry, A., and Beauchamp, B., 2008, Sverdrup basin, *in* Miall, A., ed., Sedimentary Basins of the World: The Sedimentary Basins of the United States and Canada, Volume 5: Amsterdam, The Netherlands, Elsevier, p. 451–471.

Gehling, J.G., and Droser, M.L., 2009, Textured organic surfaces associated with the Ediacara biota in South Australia: Earth-Science Reviews, v. 96, p. 196–206, https://doi.org/10.1016/j.earscirev.2009.03.002.

Grasby, S.E., and Beauchamp, B., 2008, Intrabasin variability of the carbon-isotope record across the Permian–Triassic transition, Sverdrup Basin, Arctic Canada: Chemical Geology, v. 253, p. 141–150, https://doi.org/10.1016/j.chemgeo.2008.05.005.

Grasby, S.E., Beauchamp, B., Embry, A., and Sanei, H., 2013, Recurrent Early Triassic ocean anoxia: Geology, v. 41, p. 175–178, https://doi.org/10.1130/G33599.1.

Grasby, S.E., Beauchamp, B., Bond, D.P.G., Wignall, P.B., Talavera, C., Galloway, J.M., Piepjohn, K., Reinhardt, L., and Blomeier, D., 2015, Progressive environmental deterioration in northwestern Pangea leading to the latest Permian extinction: Geological Society of America Bulletin, v. 127, p. 1331–1347, https://doi.org/10.1130/B31197.1.

Grasby, S.E., Beauchamp, B., and Knies, J., 2016, Early Triassic productivity crises delayed recovery from world's worst mass extinction: Geology, v. 44, p. 779–782, https://doi.org/10.1130/G38141.1.

Hagadorn, J.W., and Bottjer, D.J., 1999, Restriction of a Late Neoproterozoic biotope: Suspect-microbial structures and trace fossils at the Vendian-Cambrian transition: Palaios, v. 14, p. 73–85, https://doi.org/10.2307/3515362.

Hallam, A., 1991, Why was there a delayed radiation after the end-Palaeozoic extinctions?: Historical Biology, v. 5, p. 257–262, https://doi.org/10.1080/10292389109380405.

Hofmann, R., Goudemand, N., Wasmer, M., Bucher, H., and Hautmann, M., 2011, New trace fossil evidence for an early recovery signal in the aftermath of the end-Permian mass extinction: Palaeogeography, Palaeoclimatology, Palaeoecology, v. 310, p. 216–226, https://doi.org/10.1016/j.palaeo.2011.07.014.

Hofmann, R., Buatois, L.A., MacNaughton, R.B., and Mángano, M.G., 2015, Loss of the sedimentary mixed layer as a result of the end-Permian extinction: Palaeogeography, Palaeoclimatology, Palaeoecology, v. 428, p. 1–11, https://doi.org/10.1016/j.palaeo.2015.03.036.

Horacek, M., Brandner, R., and Abart, R., 2007, Carbon isotope record of the P/T boundary and the Lower Triassic in the Southern Alps: Evidence for rapid changes in storage of organic carbon: Palaeogeography, Palaeoclimatology, Palaeoecology, v. 252, p. 347–354, https://doi.org/10.1016/j.palaeo.2006.11.049.

Korte, C., and Kozur, H.W., 2010, Carbon-isotope stratigraphy across the Permian–Triassic boundary: A review: Journal of Asian Earth Sciences, v. 39, p. 215–235, https://doi.org/10.1016/j.jseaes.2010.01.005.

Knaust, D., 2010, The end-Permian mass extinction and its aftermath on an equatorial carbonate platform: Insights from ichnology: Terra Nova, v. 22, p. 195–202, https://doi.org/10.1111/j.1365-3121.2010.00934.x.

Mata, S.A., and Bottjer, D.J., 2009, The paleoenvironmental distribution of Phanerozoic wrinkle structures: Earth-Science Reviews, v. 96, p. 181–195, https://doi.org/10.1016/j.earscirev.2009.06.001.

McCave, I.N., 1970, Deposition of fine-grained suspended sediment from tidal currents: Journal of Geophysical Research. Oceans and Atmospheres, v. 75, p. 4151–4159, https://doi.org/10.1029/JC075i021p04151.

Midwinter, D., Hadlari, T., and Dewing, K., 2017, Lower Triassic river-dominated deltaic successions from the Sverdrup Basin, Canadian Arctic: Palaeogeography, Palaeoclimatology: Palaeoecology, v. 476, p. 55–67, https://doi.org/10.1016/j.palaeo.2017.03.017.

Mulder, T., Syvitski, J.P.M., Migeon, S., Faugères, J.-C., and Savoye, B., 2003, Marine hyperpycnal flows: Initiation, behaviour and related deposits. A review: Marine and Petroleum Geology, v. 20, p. 861–882, https://doi.org/10.1016/j.marpetgeo.2003.01.003.

Noffke, N., 2000, Extensive microbial mats and their influences on the erosional and depositional dynamics of a siliciclastic cold water environment (Lower Arenigian, Montagne Noire, France): Sedimentary Geology, v. 136, p. 207–215, https://doi.org/10.1016/S0037-0738(00)00098-1.

Noffke, N., 2010, Microbial Mats in Sandy Deposits from the Archean Era to Today: Heidelberg, Germany, Springer, 194 p.

Noffke, N., Gerdes, G., Klenke, T., and Krumbein, W.E., 2001, Microbially induced sedimentary structures: A new category within the classification of primary sedimentary structures: Journal of Sedimentary Research, v. 71, p. 649–656, https://doi.org/10.1306/2DC4095D-0E47-11D7-8643000102C1865D.

Noffke, N., Knoll, A.H., and Grotzinger, J.P., 2002, Sedimentary controls on the formation and preservation of microbial mats in siliciclastic deposits: A case study from the Upper Neoproterozoic Nama Group, Namibia: Palaios, v. 17, p. 533–544, https://doi.org/10.1669/0883-1351(2002)017<0533:SCOTFA>2.0.CO;2.

Pflüger, F., 1999, Matground structures and redox facies: Palaios, v. 14, p. 25–39, https://doi.org/10.2307/3515359.

Pietsch, C., Mata, S.A., and Bottjer, D.J., 2014, High temperature and low oxygen perturbations drive contrasting benthic recovery dynamics following the end-Permian mass extinction: Palaeogeography, Palaeoclimatology, Palaeoecology, v. 399, p. 98–113, https://doi.org/10.1016/j.palaeo.2014.02.011.

Porada, H., and Bouougri, E., 2007, 'Wrinkle structures'—a critical review, *in* Schieber, J., Bose P., Eriksson, P.G., Banerjee, S., Sarkar, S., Altermann, W., and Catuneanu, O., eds., Atlas of Microbial Features Preserved within the Siliciclastic Rock Record, Volume 2: Amsterdam, The Netherlands, Elsevier, p. 135–188.

Proemse, B.C., Grasby, S.E., Wieser, M.E., Mayer, B., and Beauchamp, B., 2013, Molybdenum isotope evidence for oxic marine conditions during the Latest Permian Extinction: Geology, v. 41, p. 967–970, https://doi.org/10.1130/G34466.1.

Pruss, S., Fraiser, M., and Bottjer, D.J., 2004, Proliferation of Early Triassic wrinkle structures: Implications for environmental stress following the end-Permian mass extinction: Geology, v. 32, p. 461–464, https://doi.org/10.1130/G20354.1.

Pruss, S., Fraiser, M., and Bottjer, D.J., 2005, The unusual sedimentary rock record of the Early Triassic: A case study from the southwestern United States: Palaeogeography, Palaeoclimatology, Palaeoecology, v. 222, p. 33–52, https://doi.org/10.1016/j.palaeo.2005.03.007.

Reineck, H.E., and Wunderlich, F., 1968, Classification and origin of flaser and lenticular bedding: Sedimentology, v. 11, p. 99–104, https://doi.org/10.1111/j.1365-3091.1968.tb00843.x.

Song, H.J., Wignall, P.B., Tong, J.N., and Yin, H.F., 2013, Two pulses of extinction during the Permian-Triassic crisis: Nature Geoscience, v. 6, p. 52–56, https://doi.org/10.1038/ngeo1649.

Steel, E., Simms, A.R., Warrick, J., and Yokoyama, Y., 2016, Highstand shelf fans: The role of buoyancy reversal in the deposition of a new type of shelf sand body: Geological Society of America Bulletin, v. 128, p. 1717–1724, https://doi.org/10.1130/B31438.1.

Tozer, E.T., 1965, Lower Triassic stages and ammonoid zones of Arctic Canada: Geological Survey of Canada Paper 65-12, 14 p., https://doi.org/10.4095/100985.

Tozer, E.T., 1967, A standard for Triassic time: Geological Survey of Canada Bulletin, v. 156, 141 p., https://doi.org/10.4095/101452.

Tribovillard, N., Algeo, T.J., Lyons, T., and Riboulleau, A., 2006, Trace metals as paleoredox and paleoproductivity proxies: An update: Chemical Geology, v. 232, p. 12–32, https://doi.org/10.1016/j.chemgeo.2006.02.012.

Twitchett, R.J., 2006, The palaeoclimatology, palaeoecology and palaeoenvironmental analysis of mass extinction events: Palaeogeography, Palaeoclimatology, Palaeoecology, v. 232, p. 190–213, https://doi.org/10.1016/j.palaeo.2005.05.019.

Twitchett, R.J., and Wignall, P.B., 1996, Trace fossils and the aftermath of the Permo-Triassic mass extinction: Evidence from northern Italy: Palaeogeography, Palaeoclimatology, Palaeoecology, v. 124, p. 137–151, https://doi.org/10.1016/0031-0182(96)00008-9.

Vennin, E., Olivier, N., Brayard, A., Bour, I., Thomazo, C., Escarguel, G., Fara, E., Bylund, K.G., Jenks, J.F., Stephen, D.Q., and Hofmann, R., 2015, Microbial deposits in the aftermath of the end-Permian mass extinction: A diverging case from the Mineral Mountains (Utah, USA): Sedimentology, v. 62, p. 753–792, https://doi.org/10.1111/sed.12166.

Wignall, P.B., 1994, Black Shales: Oxford, UK, Oxford University Press, 144 p.

Wignall, P.B., and Twitchett, R.J., 1999, Unusual intraclastic limestones in Lower Triassic carbonates and their bearing on the aftermath of the end Permian mass extinction: Sedimentology, v. 46, p. 303–316, https://doi.org/10.1046/j.1365-3091.1999.00214.x.

Wignall, P.B., Morante, R., and Newton, R., 1998, The Permo-Triassic transition in Spitsbergen: $\delta^{13}C_{org}$ chemostratigraphy, Fe and S geochemistry, facies, fauna and trace fossils: Geological Magazine, v. 135, p. 47–62, https://doi.org/10.1017/S0016756897008121.

Wignall, P.B., Bond, D.P.G., Kuwahara, K., Kakuwa, Y., Newton, R.J., and Poulton, S.W., 2010, An 80 million year oceanic redox history from Permian to Jurassic pelagic sediments of the Mino-Tamba terrane, SW Japan, and the origin of four mass extinctions: Global and Planetary Change, v. 71, p. 109–123, https://doi.org/10.1016/j.gloplacha.2010.01.022.

Wignall, P.B., Bond, D.P.G., S un, Y.D., Grasby, S.E., Beauchamp, B., Joachimski, M.M., and Blomeier, D.P.G., 2016, Ultra-shallow-marine anoxia in an Early Triassic shallow-marine clastic ramp (Spitsbergen) and the suppression of benthic radiation: Geological Magazine, v. 153, p. 316–331, https://doi.org/10.1017/S0016756815000588.

Wilkin, R.T., and Barnes, H.L., 1997, Formation processes of framboidal pyrite: Geochimica et Cosmochimica Acta, v. 61, p. 323–339, https://doi.org/10.1016/S0016-7037(96)00320-1.

Wilkin, R.T., Barnes, H.L., and Brantley, S.L., 1996, The size distribution of framboidal pyrite in modern sediments: An indicator of redox conditions: Geochimica et Cosmochimica Acta, v. 60, p. 3897–3912, https://doi.org/10.1016/0016-7037(96)00209-8.

Wilson, R.D., and Schieber, J., 2014, Muddy prodeltaic hyperpycnites in the lower Genesee Group of central New York, USA: Implications for mud transport in epicontinental seas: Journal of Sedimentary Research, v. 84, p. 866–874, https://doi.org/10.2110/jsr.2014.70.

Woods, A.D., Bottjer, D.J., and Corsetti, F.A., 2007, Calcium carbonate seafloor precipitates from the outer shelf to slope facies of the Lower Triassic (Smithian-Spathian) Union Wash Formation, California, USA: Sedimentology and palaeobiologic significance: Palaeogeography, Palaeoclimatology, Palaeoecology, v. 252, p. 281–290, https://doi.org/10.1016/j.palaeo.2006.11.053.

Zavala, C., Arcuri, M., Meglio, M.D., Diaz, H.G., and Contreras, C., 2011, A genetic facies tract for the analysis of sustained hyperpycnal flow deposits, *in* Slatt, R.M., and Zavala, C., eds., Sediment transfer from shelf to deep water: Revisiting the delivery system: American Association of Petroleum Geologists, Studies in Geology 61, p. 31–51.

Science Editor: Rob Strachan
Associate Editor: William Clyde

Manuscript Received 8 January 2019
Revised Manuscript Received 15 May 2019
Manuscript Accepted 20 June 2019

Printed in the USA